Received: 8 September 2024 | Revised: 18 November 2024 | Accepted: 22 November 2024

DOI: 10.1111/joa.14193

Journal of Anatomy ANATOMICAL SOCIETY WILEY

ORIGINAL ARTICLE

Histological analysis of retinal development and remodeling in the brown anole lizard (*Anolis sagrei*)

Ashley M. Rasys[1] | Shana H. Pau[2] | Katherine E. Irwin[1] | Sherry Luo[2] | Hannah Q. Kim[1] | M. Austin Wahle[2] | Douglas B. Menke[2] | James D. Lauderdale[1,3]

[1]Department of Cellular Biology, The University of Georgia, Athens, Georgia, USA

[2]Department of Genetics, The University of Georgia, Athens, Georgia, USA

[3]Neuroscience Division of the Biomedical and Translational Sciences Institute, The University of Georgia, Athens, Georgia, USA

Correspondence
James D. Lauderdale, Department of Cellular Biology, University of Georgia, Athens, GA 30602, USA.
Email: jdlauder@uga.edu

Douglas B. Menke, Department of Genetics, University of Georgia, Athens, GA 30602, USA.
Email: dmenke@uga.edu

Funding information
National Science Foundation, Grant/Award Number: 1149453 and 1827647; Achievement Rewards for College Scientists Foundation; Society for Developmental Biology Emerging Models; National Institute of General Medical Sciences, Grant/Award Number: T32GM007103; ARCS Foundation Scholarship

Abstract

The fovea, a pit in the retina, is crucial for high-acuity vision in humans and is found in the eyes of other vertebrates, including certain primates, birds, lizards, and fish. Despite its importance for vision, our understanding of the mechanisms involved in fovea development remains limited. Widely used ocular research models lack a foveated retina, and studies on fovea development are mostly limited to histological and molecular studies in primates. As a first step toward elucidating fovea development in nonprimate vertebrates, we present a detailed histological atlas of retina and fovea development in the bifoveated *Anolis sagrei* lizard, a novel reptile model for fovea research. We test the hypothesis that retinal remodeling, leading to fovea formation and photoreceptor cell packing, is related to asymmetric changes in eye shape. Our findings show that anole retina development follows the typical spatiotemporal patterning observed in most vertebrates: retinal neurogenesis starts in the central retina, progresses through the temporal retina, and finishes in the nasal retina. However, the areas destined to become the central or temporal fovea differentiate earlier than the rest of the retina. We observe dynamic changes in retinal thickness during ocular elongation and retraction—thinning during elongation and thickening during retraction. Additionally, a transient localized thickening of the ganglion cell layer occurs in the temporal fovea region just before pit formation. Our data indicate that anole retina development is similar to that of humans, including the onset and progression of retinal neurogenesis, followed by changes in ocular shape and retinal remodeling leading to pit formation. We propose that anoles are an excellent model system for fovea development research.

KEYWORDS
fovea, lizard, neurogenesis, retinal remodeling, spatiotemporal patterning

1 | INTRODUCTION

For centuries, physicians and researchers alike have been captivated by the eye and have sought to understand the pathways that enable sight. As a result, decades of work have centered around investigating the development of the human retina. Discovered by Samuel Thomas von Sömmerring in the early 1800s, the fovea is a pit located in the macular region of the human eye (Barber, 1955; Mann, 1928) and has long been thought to be a critical feature for high visual acuity in humans as well as certain other vertebrates (Slonaker, 1897). Although present in some species of birds (Fite & Rosenfield-Wessels, 1975; Walls, 1942), lizards (Hulke, 1866; Röll, 2001; Underwood, 1970; Walls, 1942), and fish (Collin, 1999; Easter Jr., 1992), much of our understanding of fovea development comes from work in foveated primates (Hendrickson, 1992, 2005, 2015; Hendrickson et al., 2012; Hendrickson & Drucker, 1992; Hendrickson & Kupfer, 1976; Hendrickson & Provis, 2006; Hendrickson & Yuodelis, 1984; Peng et al., 2019; Springer & Hendrickson, 2004a, 2004b, 2005; Voigt et al., 2019; Yan et al., 2020; Yuodelis & Hendrickson, 1986). This body of work includes histological studies of the primate eye that have provided important insights into the timing and progression of retina development and foveal morphogenesis. The primate fovea initially develops through the lateral displacement of the retina's ganglion cell layer (GCL) and inner nuclear layer (INL) (Hendrickson et al., 2012; Hendrickson & Yuodelis, 1984). Over time, the photoreceptor cells, which make up the entire outer nuclear layer (ONL), move and pack in around the foveal center (Hendrickson et al., 2012; Hendrickson & Drucker, 1992; Hendrickson & Yuodelis, 1984; Yuodelis & Hendrickson, 1986).

Currently, the underlying developmental mechanisms involved in reshaping the retinal landscape remain poorly understood. Additionally, it is unclear how specific retinal regions are instructed to develop a fovea. Addressing these questions requires the ability to manipulate gene function or disrupt cell signaling pathways implicated in fovea development. This is challenging in primates due to their reproduction schedule, generation time, and ethical concerns regarding genome modification and raising of mutant lines. Determining the mechanisms involved in pit formation is also not feasible in other commonly used animal models for eye research, such as mice, chicks, *Xenopus*, and zebrafish, because they all lack a foveated retina. Hence, there is a need for a new foveated model system that can be easily reared in a laboratory setting, reproduces frequently, has a short generation time, and whose genome can be easily edited. To address this need, we are developing the brown anole lizard (*Anolis sagrei*) as a foveated model system for research (Rasys, Divers, et al., 2019; Rasys, Park, et al., 2019; Rasys, Pau, Irwin, Luo, Kim, et al., 2021; Rasys, Pau, Irwin, Luo, Menke, et al., 2021).

The retina of *Anolis sagrei*, and other anole lizards, possesses both a prominent, funnel-shaped central fovea and a shallower temporal fovea (Fite & Lister, 1981; Makaretz & Levine, 1980; Rasys, Pau, Irwin, Luo, Kim, et al., 2021; Sannan et al., 2018; Underwood, 1970; Walls, 1942). This deep central fovea lacks all retina cell layers at its center, while the shallower temporal fovea retains all these cell layers. Although among reptiles the presence of a deep central fovea and a second, shallower temporal fovea is unique to anoles, this arrangement is commonly found in birds (Bringmann, 2019; Underwood, 1970; Walls, 1942). All other foveated lizards that have been examined possess a single fovea located in the central retina (Underwood, 1970) or, in the case of geckos, a single fovea located in the temporal region of the retina (Röll, 2001). While the central fovea is thought to provide high visual acuity for detecting distant objects (Bringmann, 2019; Fleishman, 2024; Locket, 1992), the temporal fovea is thought to enhance depth perception, which is particularly useful for prey capture (Fleishman, 2024; Mitkus et al., 2018). The dual foveal system is postulated to allow anoles to have sharp vision in both the lateral and frontal visual fields, aiding in their predatory behavior (Fleishman, 2024). Studies of foveal development in *A. sagrei* are expected to provide insights into the cellular and molecular mechanisms underlying fovea formation and retinal remodeling.

Remarkably, during embryonic development, anole eyes undergo dynamic changes in their ocular shape (Rasys, Pau, Irwin, Luo, Kim, et al., 2021). First, the eye dramatically elongates in the regions that will develop a fovea. This is followed by a retraction period, where the eye returns back to its original spherical shape. It is during this retraction phase that the foveae develop. We previously proposed that remodeling of the retina landscape results from changes in eye shape, eventually leading to the organization of high visual acuity areas (Rasys, Pau, Irwin, Luo, Kim, et al., 2021). Here, we test this hypothesis by carefully examining the morphology of the retina prior to, during, and after ocular elongation.

2 | METHODS

2.1 | Animals

Lizards are maintained in a laboratory breeding colony at the University of Georgia following the anole husbandry and care recommendations outlined by Sanger, Hime, et al. (2008). Eggs were maintained in the lab following the protocol described by Rasys, Pau, Irwin, Luo, Kim, et al. (2021). Experiments included both male and female lizard embryos as well as hatchlings. Hatchlings were euthanized according to the American Veterinary Medical Association (AVMA) Guidelines for the Euthanasia of Animals (Association AVM, 2020; Conroy et al., 2009). All experiments were approved, performed, and overseen by the University of Georgia Institutional Animal Care and Use Committee in accordance with the National Institutes of Health Guide for the Care and Use of Laboratory Animals.

2.2 | Staging and dissection

Anole embryos develop over a 30–33 day period when incubated at 28°C. Embryos were collected from eggs at various timepoints after

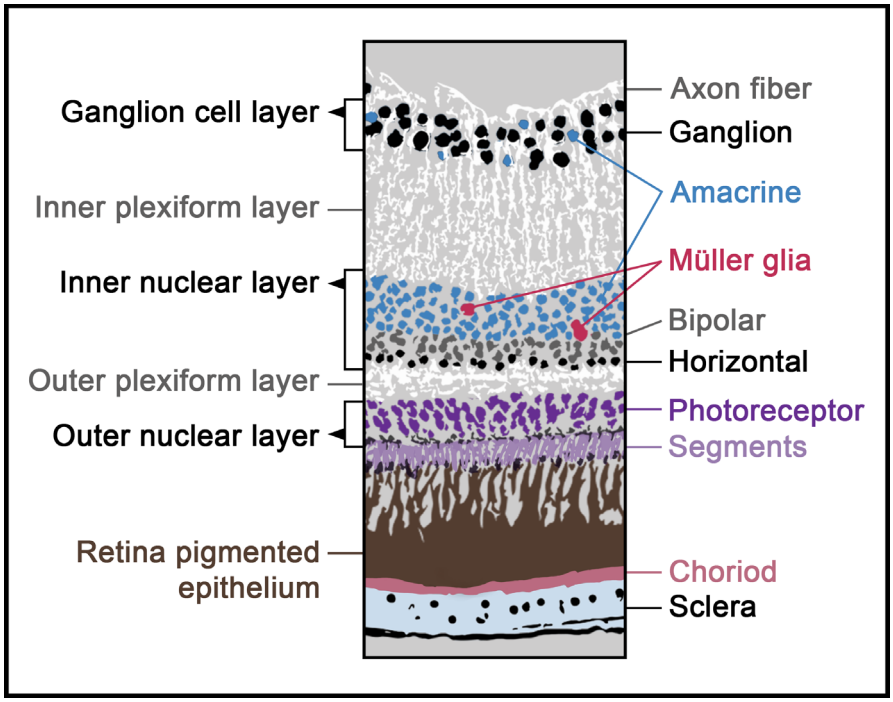

FIGURE 1 Diagram of cell organization in the adult brown anole lizard retina.

egg lay and removed from their egg shells following the protocol described by Rasys, Pau, Irwin, Luo, Kim, et al. (2021). Embryos were staged according to the guidelines by Sanger, Losos, et al. (2008). Eyes were collected from 4 or more embryos from each developmental stage.

2.3 | Fixation, embedding, and staining

After dissection, the eyes were placed in Bouin's fixative, chosen over 4% Paraformaldehyde (PFA) solution due to its superior ability to maintain ocular shape and resist shrinkage artifacts during the dehydration process. Additionally, it was selected for its quality in preserving individual cell morphology, enabling easy detection of mitotic, differentiating, and pyknotic cells on histological sections. The eyes were fixed at 4°C overnight on a rocker and then rinsed the next day in 1× phosphate-buffered saline (137 mM NaCl, 2.7 mM KCl, 10 mM Na_2HPO_4, 1.8 mM KH_2PO_4, pH 7.4) with five 15-min washes. They were then dehydrated in a series of graded ethanol solutions (70%, 80%, 90%, 96%, and 100% twice) for 15 min each. After dehydration, the eyes were soaked in xylene for 30 min and incubated in a series of three paraffin wax jars for 30 min at 65°C. The eyes were embedded in paraffin, serially sectioned along the horizontal plane at a 10 μm thickness, stained, and mounted following standard hematoxylin and eosin (H&E) and Cytoseal (Thermo Scientific™ Richard-Allan Scientific™) protocols. The sections were imaged using a KEYENCE BZ-700 microscope, and photomosaic images were generated with Keyence image stitching software. Contrast and white balance of images were digitally enhanced using Adobe Photoshop CC (2017.01 release).

2.4 | Retina measurements

Retina measurements were performed on horizontally sectioned eyes from stage 6 ($n = 4$), stage 14 ($n = 4$), and hatchling ($n = 6$) lizards following our approach published in Wahle et al. (2023). Total outer and inner retinal lengths were measured, and the mean plus standard deviation was recorded for each section. The outer and inner retina lengths were divided into 10 individual bins, with each foveal region centered in a bin. Retinal width measurements (13 different areas) were taken at the intersection of the bins, the foveal center, and parafoveal regions. This approach ensured consistent sampling of the same regions across multiple embryo retinas and stages. Retina length and width were recorded in micrometer (μm) units.

3 | RESULTS

3.1 | Structure of the adult retina

The results of this study reference the retinal structure of the adult anole, as depicted in this sketch modeled on histological sections cut through anole eyes (Figure 1). This retinal structure is similar to that of other vertebrates. The ganglion cell layer (GCL) consists of ganglion cells and putative displaced amacrine cells. The inner nuclear layer (INL) contains amacrine cells, bipolar cells, Müller glia, and horizontal cells, while the outer nuclear layer (ONL) is populated by photoreceptor cells. The inner plexiform layer, located between the GCL and INL, consists of synaptic connections between neurons in these two layers. Similarly, the outer plexiform layer (OPL), located between the INL and ONL, consists of synaptic connections between bipolar

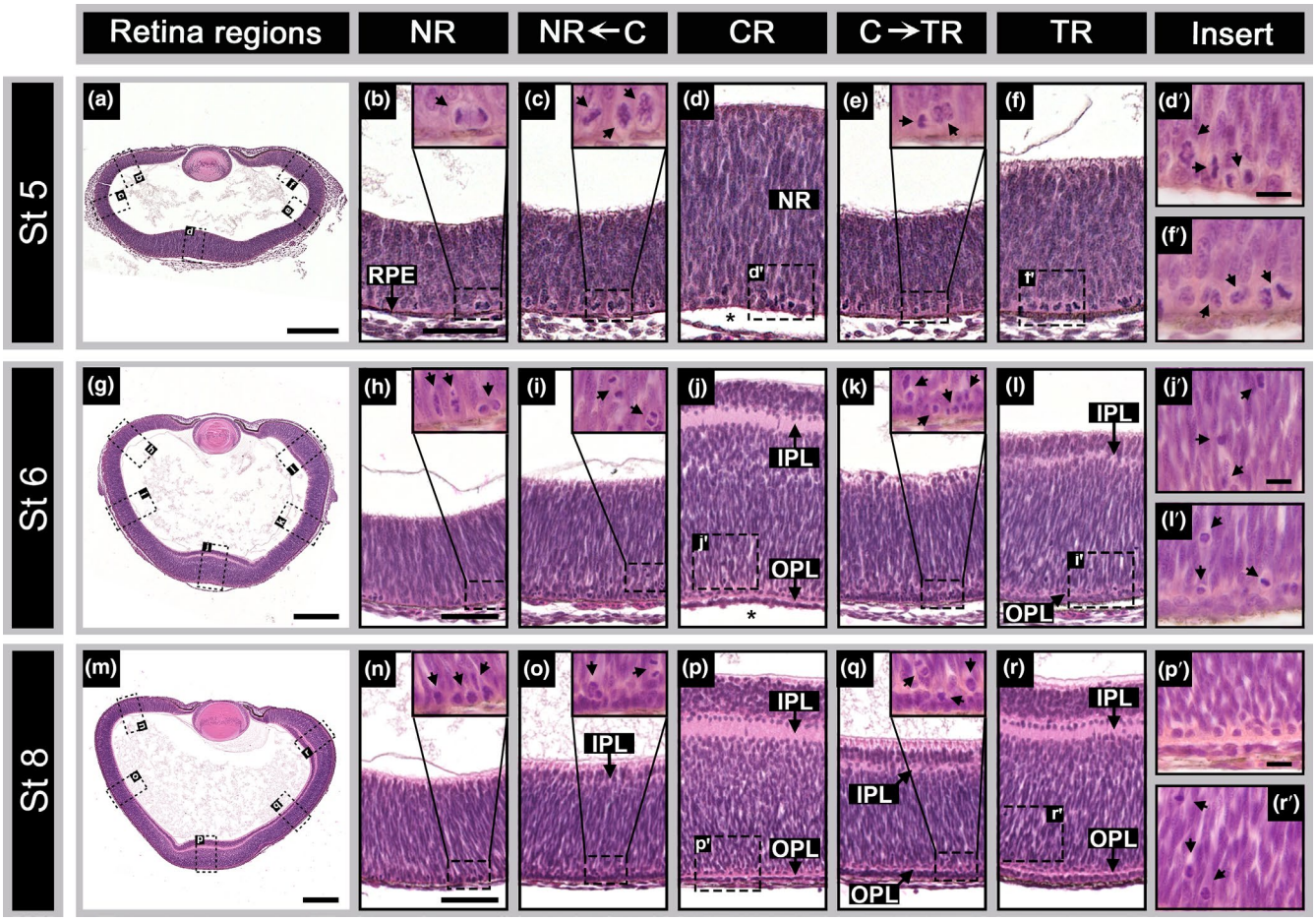

FIGURE 2 Foveal areas in anoles have retina mounding and undergo retinal lamination before the rest of the retina. Side panels show H&E-stained horizontal sections of stage 5 (a), stage 6 (g), and stage 8 (m) embryos. The retina areas: NR—nasal retina (b, h, and n), NR←C—area between the central and nasal retina (c, i, and o), CR—central retina (d, j, and p), C→TR—area between the central and temporal retina (e, k, and q), and TR—temporal (f, l, and r) are shown for each (a), (g), and (m) sections. Magnified inserts of the foveal regions are shown for stage 5 (d' and f'), stage 6 (j' and l'), and stage 8 (p' and r') embryos. Images (b–f, h–l, and n–r) and (d'–f', j'–l', and p'–r') are respectively to scale with one another. Markers: Black arrows—mitotic cells; RPE—retinal pigmented epithelium; NR—neural retina; IPL—inner plexiform layer; OPL—outer plexiform layer; scale bars—250 μm (a, g, and m), 50 μm (b–f, h–l, and n–r), and 20 μm (d'–f', j'–l', and p'–r').

cells, horizontal cells, and photoreceptors. Immediately adjacent to the ONL on the posterior side of the eye is the retinal pigmented epithelium (RPE). The RPE is a single-cell layer with an extensive array of microvilli extending from its apical surface, interdigitating with the outer segments of the photoreceptors. Adjacent to the RPE is the heavily vascularized choroid and cartilaginous sclera, which form the tough outer surface of the ocular globe.

3.2 | Early retinal development of foveal areas

In the early developing eye of stage 5 embryos, the prospective central and temporal foveal regions of the neural retina exhibit a thickened, mound-like appearance when compared to adjacent regions (Figure 2a–f; compare regions d and f to b, c, and e). These observations suggest that the regions of the retina that will give rise to the central and temporal fovea are further along in development than non-foveated retinal regions.

3.3 | Cell proliferation and retina lamination

During the period that immediately follows optic cup formation in the developing anole (Sanger stages 1–3; Sanger, Losos, et al., 2008), mitotic cells are distributed throughout the developing neural retina adjacent to the retinal pigmented epithelium (data not shown; see fig. 2 of Rasys, Pau, Irwin, Luo, Menke, et al. (2021)). By late stage 3, an increase in the number of dividing cells in the central region of the retina is observed. By stage 4, a slight mounding of the retina (i.e., increased neural retina thickness localized to a specific area of the retina) is detected centrally (data not shown; see *Anolis Eye Development* poster from Rasys, Pau, Irwin, Luo, Kim, et al., 2021). As the embryo enters stage 5 of development, the eye has grown considerably in overall size, and regional differences in both morphology and the numbers of mitotic figures become evident (Figure 2a–f). Retinal mounding in the central retina increases in both area and thickness, and a similar, but somewhat smaller, mounded formation is also observed in

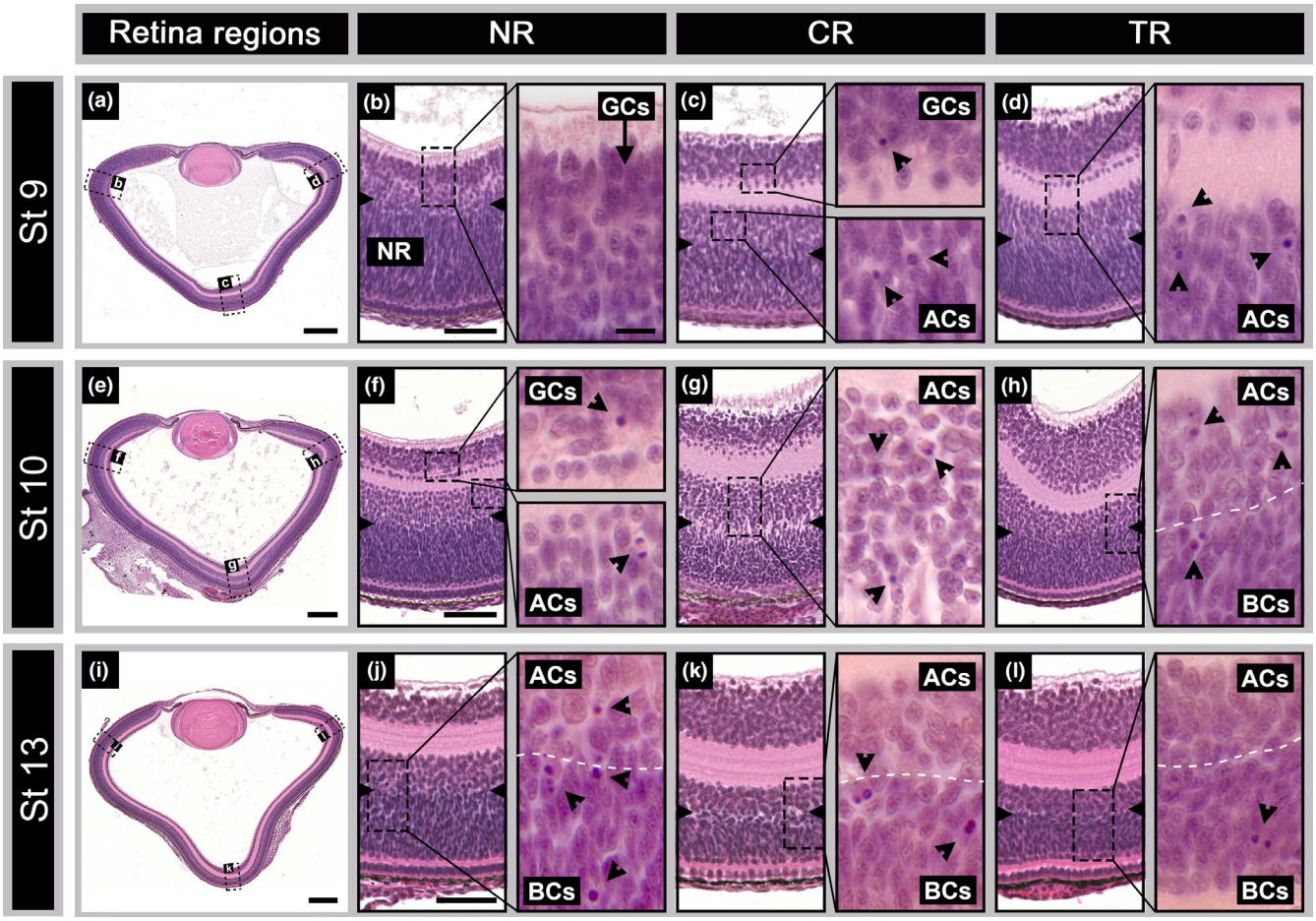

FIGURE 3 Retinal development in midstage embryos. Panels to the left show horizontal H&E-stained sections of stage 9 (a), stage 10 (e), and stage 13 (i) embryos. The nasal retina is depicted in (b, f, and j), the central retina in (c, g, and k), and temporal retina in (d, h, and l). Markers: Black arrows—presumptive horizontal cells; black arrow heads—pyknotic cells; side notches—presumptive amacrine/bipolar boundary; NR—neural retina; GCs—ganglion cells; Acs—amacrine cells; BCs—bipolar cells; dashed white lines—presumptive amacrine/bipolar boundary; and scale bars—250 μm (a, e, and i), 50 μm (b–l), and 20 μm (magnified inserts). Inserts are all to scale with each other.

the temporal region where the presumptive temporal fovea will develop (Figure 2a,d,f). The highest densities of mitotically active cells are in the mounded regions of the central and temporal retina (Figure 2a,d,f), with lower densities in the nasal peripheral retina (Figure 2a–c) and the retinal area between the central and temporal mounded regions (Figure 2a,e). Most of the mitotic figures observed in the neural retina are consistent with vertically oriented cell division (the plane of cell division was perpendicular to the plane of the neuroepithelium). In the mounded area of the central retina, horizontally dividing cells are also observed (Figure 2d).

The first signs of retinal lamination are observed by stage 6. A prominent inner plexiform layer (IPL) and developing outer plexiform layer (OPL) are found centrally, while temporally, both plexiform layers are present but less well developed (Figure 2g,j,l). Strikingly, lamination is neither evident between the central and temporal retina regions (Figure 2k) nor observed in the temporal anterior margin. This indicates that areas with retinal thickening have progressed further in development compared to other regions of the retina. During this period, cell proliferation has largely ceased in the central retina and is greatly reduced in the temporal retina. The few cells still undergoing mitosis within these areas are located distally from the ventricle surface (Figure 2j,j',l,l'). In contrast, the densities of mitotic figures in the peripheral retina and the region between the central and temporal foveal areas of stage 6 embryos are higher compared to those in stage 5 embryos. In these areas, dividing cells are mostly located adjacent to the ventricle surface (Figure 2h,l,k), but distally located mitotic cells are observed in portions of the peripheral retina starting to form neuropil (Figure 2i,k).

By stage 8, the IPL and OPL are observed in the retina between the central and temporal areas but do not extend to the temporal anterior margin (Figure 2m–r). At this stage, cell proliferation is largely restricted to the anterior nasal retina (Figure 2n,o). By stage 10, the IPL and OPL extend from the anterior margin on the temporal side of the eye around the retina but do not quite reach the anterior margin of the eye on the nasal side (Figure 3e).

Proliferation at this time has largely ceased. By stages 11–12, the IPL and OPL extend all the way around the retina (data not shown, but see Figure 3i for stage 13).

3.4 | Neurogenesis of retina cell types

We next sought to determine the approximate timeline for the emergence of cell types in the developing anole retina. In other vertebrates, the first retinal cells to be born are ganglion cells, followed by horizontal, amacrine, and cone photoreceptor cells. In contrast, rod photoreceptors, bipolar, and Müller glia cells differentiate later in retinal development (Coulombre, 1955; Kahn, 1974; La Vail et al., 1991; Prada et al., 1991; Rhodes, 1979; Smith et al., 2001; Weysse & Burgess, 1906). We monitored the appearance of these cell types in *A. sagrei* using morphological criteria described in other histological studies of the retina (Coulombre, 1955; O'Rahilly & Meyer, 1959; Weysse & Burgess, 1906).

As retinal cells differentiate, their morphology changes from spindle-shaped progenitor cells to round-shaped differentiated cells (Coulombre, 1955; Kahn, 1974; O'Rahilly & Meyer, 1959; Rhodes, 1979; Weysse & Burgess, 1906). In the anole, the first morphological indication of ganglion cell presence is observed starting at stage 5 in the central and temporal thickened regions of the retina. Postmitotically, these cells are large, round, and located at the vitreous surface of the neural retina (Figure 4b,c). Axon fibers extending from these cells toward the future optic stalk also become apparent. At stage 6, the GCL is clearly visible in the thickened regions of the central and temporal retina (Figures 2g,j,l and 4e,f). The GCL is 5–6 cell bodies deep in the central retina and 2–3 cells deep in the temporal retina (Figure 4e,f). Outside of these two regions, ganglion cells are present but few in number (e.g. Figure 4d). By stage 9, the GCL is approximately 7–8 cells deep in the thickened central and temporal retina and 2–3 cells deep in the retina between these two regions. Nasally, the GCL is just becoming morphologically distinct (Figure 4g). Shortly after this period, the central and temporal areas of the developing retina become notably longer, concordant with asymmetric expansion of the ocular globe along the nasotemporal and lateromedial axes compared to the dorsoventral axis (St 9–14; Rasys, Pau, Irwin, Luo, Kim, et al., 2021). This change in length is accompanied by a regional decrease in the cellular density of the neural retina, noticeable as a thinning of the GCL (Rasys, Pau, Irwin, Luo, Kim, et al., 2021). By stage 15, the ocular globe begins to retract, accompanied by regional increases in cellular density (Rasys, Pau, Irwin, Luo, Kim, et al., 2021). By the time of hatching, the GCL is 4–6 cells deep in all retinal regions except that of the central fovea, which is devoid of ganglion cells due to lateral displacement (Figure 4m–o).

Interestingly, a transient row of cells becomes distinctly visible in the IPL adjacent to the GCL during retinal development. These cells first appear in the central retina at stage 6 (Figure 2j,p), then in the temporal retina in the presumptive foveal region (Figures 2r, 3d and 4i), and finally in the nasal retina (Figures 3f and 4j). The regional appearance and subsequent disappearance of these cells correlate with the progression of retinal differentiation. The identity of these cells is currently unknown but may include ganglion cells and displaced amacrine cells.

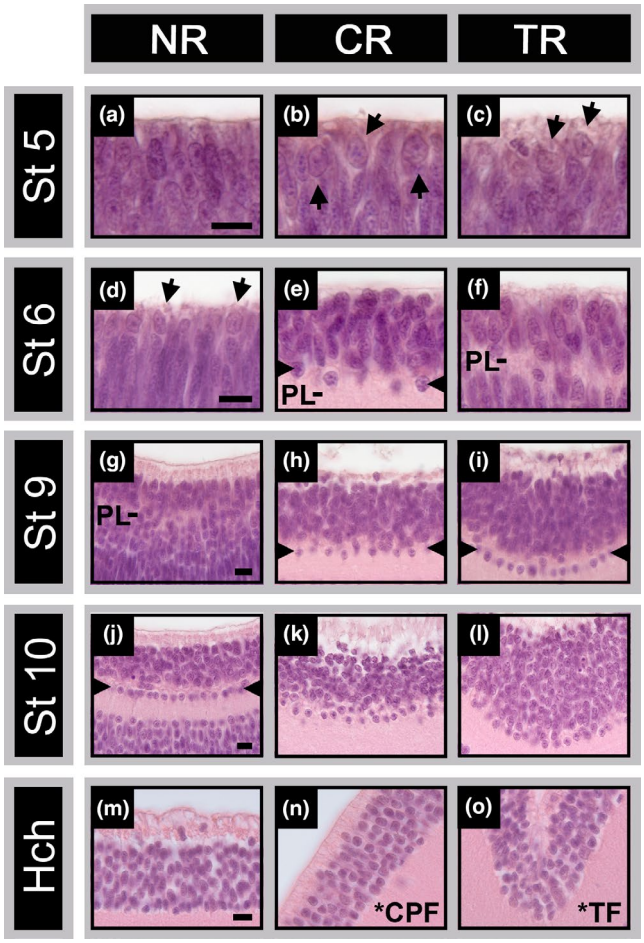

FIGURE 4 Maturation of the anole retina ganglion cell layer. Horizontal H&E-stained sections of stage 5 (a–c), stage 6 (d–f), stage 9 (f–i), and stage 10 (j–l) embryos are shown along with the hatchling (m–o). Images (a, d, g, j, and m) are from the nasal retinal region (NR), (b, e, h, k, and n) from the central region (CR), and (c, f, i, l, and o) from the temporal retina area. Images (a–c), (d–f), (g–i), (j–l), and (m–o) are to scale with each other. Markers indicate: Black arrows—presumptive ganglion cells; side notches—organized row of presumptive ganglion or displaced amacrine; PL—plexiform layer; *CPF—central parafoveal area; *TF—temporal fovea area; and scale bars—20 μm (a-o).

Amacrine cells are in the region of the INL adjacent to the IPL. Morphologically, differentiated amacrine cells are round with a larger soma than retinal progenitor cells, which exhibit a spindle-like form and are densely packed within the neural retina (Figure 3). Morphologically distinct amacrine cells first appear in small numbers in the central retina at stage 6 (Figures 2j and 5a–c), in the temporal retina by stage 7 (data not shown), and in the nasal retina by stage 9 (Figures 3a,b and 5d). The region of the INL enriched with amacrine cells can be distinguished from that enriched with bipolar somas by differences in cell density and soma morphologies. These regions are easily distinguishable from one another throughout embryonic

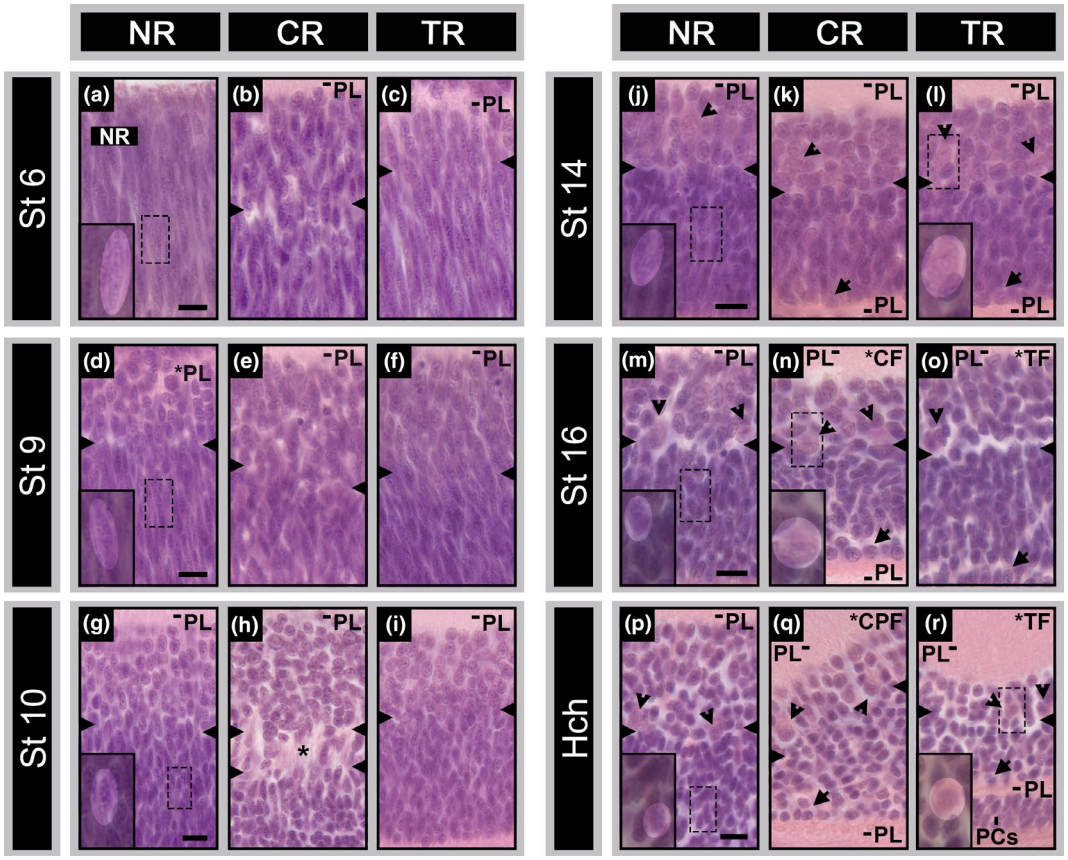

FIGURE 5 Bipolar and Müller glia histogenesis in the anole retina. Horizontal sections from embryonic stages 6 (a–c), 9 (d–f), 10 (g–i), 14 (j–l), 16 (m–o), and the hatchling (p–r) are shown. Nasal retina regions are shown in (a, d, g, j, m, and p), central retina (b, e, h, k, n, and q), and temporal retina in (c, f, i, l, o, and r). Magnified inserts in NR sections (a, d, g, j, m, and p) show presumptive bipolar cells transitioning from spindle to round morphology. Magnified inserts in CR and TR sections (l, n, and r) depict Müller glia cells. Markers: Black arrows—presumptive horizontal cells; black arrow heads—presumptive Müller glia cells; side notches—presumptive amacrine/bipolar boundary; PL—plexiform layer; asterisk—transient layer of Chievitz; *CF—central fovea; *CPF—central parafoveal region; *TF—temporal fovea; PCs—photoreceptor cells; and scale bars—20 μm (a-u). Images (a-c), (d-f), (g-i), (j-l), (m-o), and (p-r) are respectively to scale.

development and into adulthood (see Figure 3 for a clear representation). Interestingly, this boundary transiently becomes more distinct and exhibits marked separation around the presumptive fovea areas between stages 10 and 12. In this separated area, very few cell bodies are present (Figures 3e,g and 5h).

Similar to the GCL, the amacrine cell density undergoes regional changes during the periods of ocular elongation and retraction. Between stages 8 and 9, both the central and temporal regions have an amacrine cell layer that ranges from 8 to 9 cells in depth (Figure 5e,f). At the maximum extent of elongation (stage 14), this number drops to around 5 to 6 cells in depth. During retraction (stage 18), the number of cells ranges from 7 to 9 in depth throughout the retina (Figure 5j–m,p). During foveae formation in the central and temporal areas (stage 16), the amacrine cell layer progressively thins as cell bodies become laterally displaced from the foveal centers. This displacement results in an increase in cell density and retinal thickness in regions adjacent to the foveal areas. By hatching, the central fovea is completely devoid of amacrine cells, while the temporal fovea retains a layer of amacrine cells, that is, 3–4 cells deep (Figures 5r and 6).

Horizontal cells, which occupy the outermost region of the INL, and photoreceptor cells, which lie adjacent to the ventricular surface, are first observed in the central, temporal, and nasal retina areas by stages 5, 6, and 9, respectively (Figure 7b,e–g). By stage 10, the horizontal cells are neatly arranged into a single row of cells. From this point until hatching, we detect little change either in the cellular morphology or the number of horizontal cells. During this time, the ONL is largely composed of photoreceptors approximately 1–2 somas deep. Interestingly, the distance between neighboring photoreceptor cells differs between the nasal retina and the presumptive foveal areas of the central and temporal retina. In the nasal region, cells are closely packed together, while in the central and temporal regions, cells are more spaced apart (Figure 7g–o). This difference is most evident during the period of ocular elongation (stages 9–14). When the eye undergoes retraction (stages 15–18), the spacious layout of the central and temporal photoreceptor cells is lost (Figure 7p–r). By stage 14, the external limiting membrane (ELM) is present along with the first morphological indications of inner photoreceptor cell segments (Figure 7n,o). By stage 16, the number of photoreceptor cells

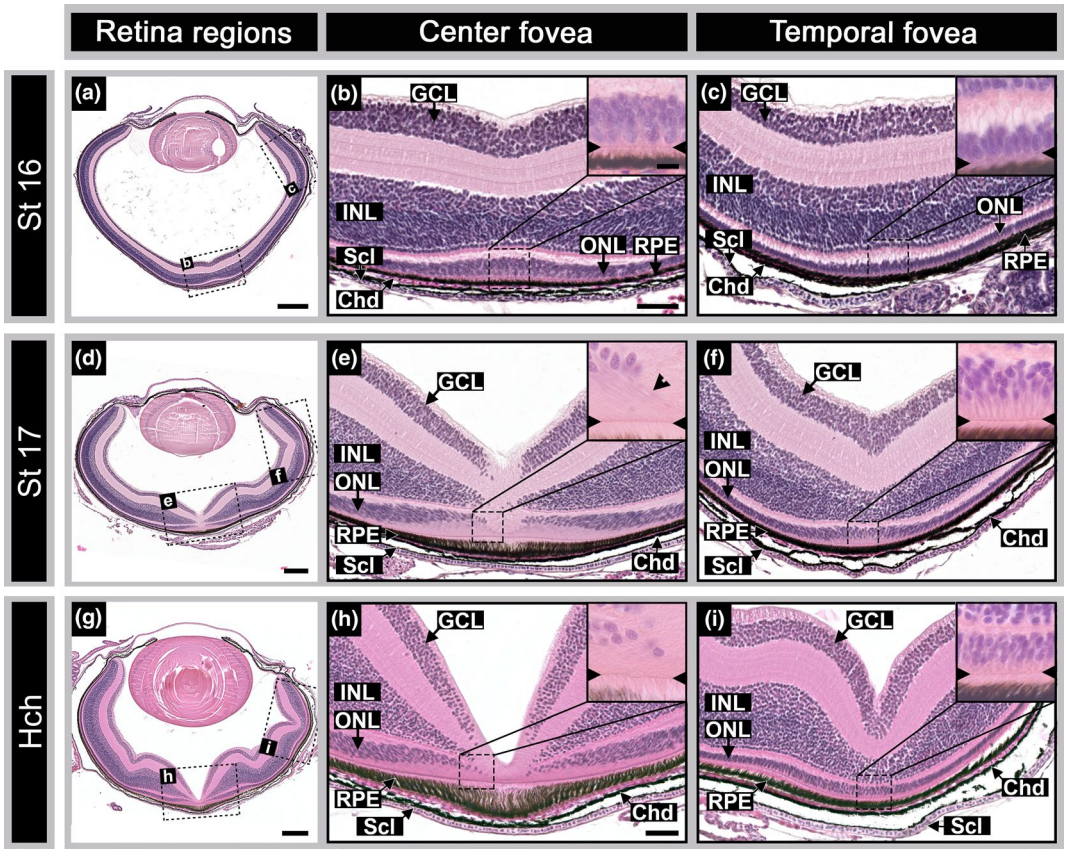

FIGURE 6 Fovea formation and photoreceptor cell packing in the anole retina. Top panels show stage 16 embryo (a–c), middle stage 17 embryo (d–f), and hatchling (g–i) horizontal H&E-stained sections. Central fovea areas are depicted in (b, e, and h), and temporal fovea regions in (c, f, and i). Magnified inserts show photoreceptor cells. Markers signify: GCL—ganglion cell layer; INL—inner nuclear layer; ONL—outer nuclear layer; RPE—retinal pigmented epithelium; Chd—choroid; Scl—sclera; side notches—external limiting membrane; and scale bars—250 μm (a, d, and g), and 50 μm (b–c, e–f, and h–i). Magnified inserts are all to scale with one another.

within the central fovea has increased from 1 to 5 cells deep; photoreceptors are 2–3 cells deep in the temporal fovea (Figure 7q,r). At the time of hatching, photoreceptor and horizontal cells present in the central fovea have become completely laterally displaced, their processes elongated, and their inner and outer segments lengthened. In contrast, in the temporal foveal center, photoreceptor cells are 4–5 cells deep, and horizontal cells are still present (Figure 7s–u).

Nestled between the amacrine and horizontal cells is a dense population of presumptive bipolar neurons. Due to the lack of definitive morphological features and the challenges associated with distinguishing cells in regions of high cell density, we present only a rough timeline of observable changes in cell morphology (i.e., the shift from spindle to round morphology) seen in a large number of cells. Presumptive bipolar cells were first detected between stages 9–10, 10, and 12 for the central, temporal, and nasal retina regions, respectively (Figure 5d–i). As development progresses, most of these presumptive bipolar cells transition from spindle to round cell morphology throughout the retina, and by stage 14, they appear largely uniform in shape (Figure 5j–l). During the formation of the central and temporal foveae (stage 16), the number of bipolar neurons decreases at the foveal centers, similar to the pattern seen with amacrine cells. By hatching, the central fovea is devoid of bipolar cells, while the temporal fovea retains bipolar cells (Figure 5m–r).

Müller glia somas tend to be larger than those of other retinal cells and are typically located in the INL, between the amacrine and bipolar somas. Müller glia nuclei are also more eosinophilic than other cells in the INL. The processes of Müller glia extend across the full thickness of the retina, reaching both the outer and inner limiting membranes. Cells matching this morphological description are first observed in small numbers between stages 11, 12, and 13 in the central, temporal, and nasal areas, respectively, and are more easily detected when the ELM appears at stage 14 (Figure 5l,n,r).

3.5 | Cell death

Naturally occurring waves of cell death, which progress in the same order as neuron birth, have been observed in other vertebrates (Beazley et al., 1987). In anoles, we found that cell death follows the same spatiotemporal pattern as neurogenesis: pyknotic cells appear first in the central retina, followed by the temporal retina, then regions immediately flanking the central retina, and lastly the

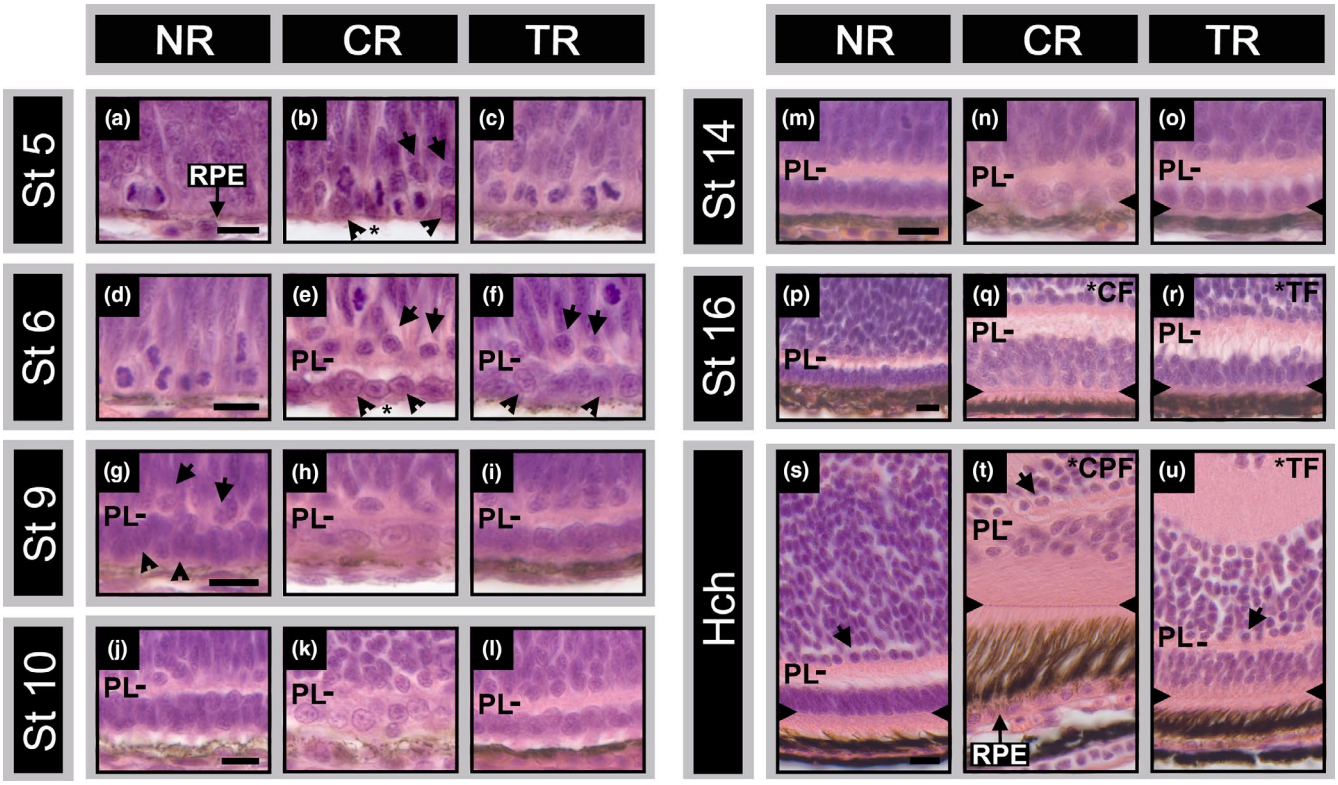

FIGURE 7 Horizontal and photoreceptor cell development in the anole retina. Images of H&E-stained horizontal sections from stage 5 (a–c), stage 6 (d–f), stage 9 (g–i), stage 10 (j–l), stage 14 (m–o), stage 16 (p–r) embryos are depicted along with the hatchling (s–u). Nasal retina regions are shown in (a, d, g, j, m, p, and s), central retina (b, e, h, k, n, q, and t), and temporal retina in (c, f, i, l, o, r, and u). Markers indicate: Black arrows—presumptive horizontal cells; black arrow heads—presumptive photoreceptor cells; side notches—external limiting membrane; RPE—retina pigmented epithelium; asterisk—RPE absent due to sectioning artifact; PL—plexiform layer; *CF—central fovea; *CPF—central parafoveal region; *TF—temporal fovea; and scale bars—20 μm (a–u). Images (a–c), (d–f), (g–i), (j–l), (m–o), (p–r), and (s–u) are to scale with one another, respectively.

nasal retina (Figure 3). Cell death is first detected within the GCL and amacrine layer as early as stage 9, becoming more prominent by stage 10 in the central and temporal areas of the retina. Although pyknotic cells are also present in these cell layers in the nasal retina at this stage, they are relatively few in number (Figure 3c,d,f–h). By stage 11, the majority of pyknotic cells in the central and temporal regions are found in the amacrine layer, whereas the bulk of dying cells in the nasal regions and areas immediately flanking the central retina are still within the GCL. This progression continues into stages 12–13, where cell death in the central and temporal retina is largely restricted to bipolar neurons. In other retinal regions, cell death is predominantly found in the amacrine layer at stage 12 and later in the bipolar region at stage 13 (Figure 3j–l). By stage 15, evidence of cell death is mostly absent from the central retina. Elsewhere, a few pyknotic cells are detected in the amacrine region of the INL in the nasal retina, and numerous pyknotic cells are observed in the bipolar region of the INL in the temporal retina. By stage 16, cell death is only detected in the nasal retina amongst bipolar neurons. At stage 17, no cell death is observed. We did not observe any obvious pyknotic cells in the photoreceptor and horizontal cell layers. Given that these cells represent a small proportion of cells in the retina, it is possible that cell death in these layers went unnoticed because fewer cell death events are occurring.

3.6 | Fovea formation and retinal remodeling

We next assessed how ocular elongation and retraction contribute to remodeling the retina, focusing on the development of the foveae. The foveae form during the last week of embryonic development in anoles, between stages 16 and 18, a period when the eye is actively undergoing ocular retraction (Rasys, Pau, Irwin, Luo, Kim, et al., 2021). As the foveae form, they do so through the lateral displacement of the retina's nuclear layers and the movement of photoceptor cells toward the foveal centers. Halfway through stage 16, the first morphological signs of foveae formation can be detected. At the central fovea, an indentation in the GCL and a pronounced increase in the number of photoreceptor cells (5 cells deep) in the ONL are observed (Figure 6a–c). By stage 17, all three nuclear layers—GCL, INL, and ONL—become laterally displaced at the central fovea. As the ONL displaces, the elongated photoreceptor cell processes and cell bodies extend approximately 45° away from the ELM at the

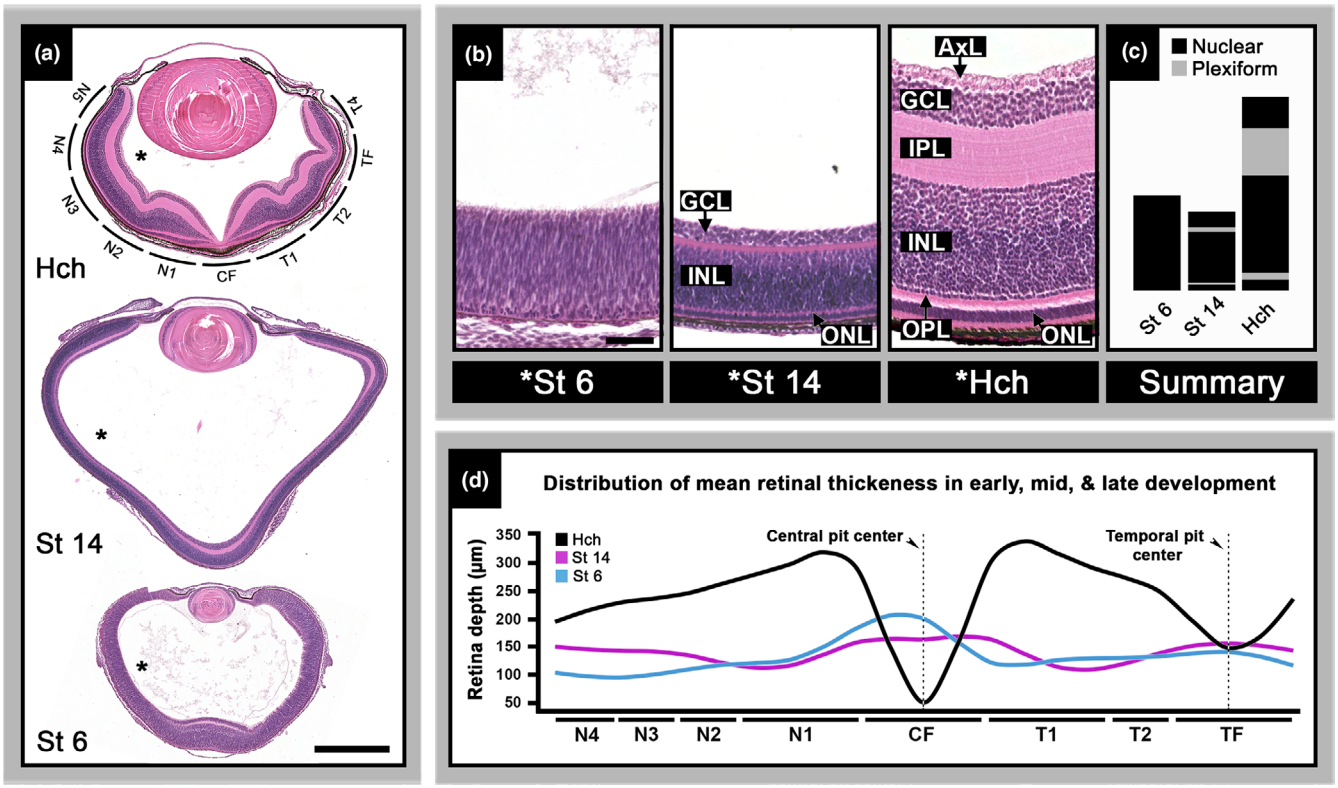

FIGURE 8 Retinal remodeling during ocular elongation and retraction. Panel (a) shows H&E-stained horizontal sections from stage 6 and 14 lizard embryos as well as the hatchling. Retinal binning is depicted around hatchling section shown in (a). Panel (b) shows retina thickness across stages 6, 14 and the hatchling taken from the nasal retina, asterisk area shown in (a). (c) is a diagram summary of (b) comparing nuclear (black) and plexiform (grey) layers. Graph (d) shows mean retina thickness and distribution across embryonic stages 6 (blue), 14 (magenta), and the hatching (black). Markers: GCL—ganglion cell layer; INL—inner nuclear layer; ONL—outer nuclear layer; IPL—inner plexiform layer; OPL—outer plexiform layer; AxL—axon layer; asterisk—retina areas shown in (b); intersection of retina bins (N5, N4, N3, N2, N1, CF, T1, T2, TF, T4)—demarks where retina width measurements were performed; and scale bars—500 µm (a) and 50 µm (b).

foveal center (Figure 6e). This lateral displacement extends well into the parafoveal region during this period. By stage 18, ocular retraction is complete, and the central fovea exhibits all of the essential characteristics present in adults.

The temporal fovea develops somewhat differently. Before a shallow pit is observed, the retina briefly increases in width, forming a slight mound or dome (Figure 6a,c). This doming of the temporal retina appears primarily due to a slight increase in the number of ganglion cells in this region. A slight increase in photoreceptor cells (2–3 cells deep) is also apparent at the foveal center. By stage 17, photoreceptors are 4–5 cells deep, the INL has narrowed, and a slight pit has formed (Figure 6f). At hatching, the temporal fovea pit is more pronounced, and the area with photoreceptor cell packing has expanded (Figure 6g,i).

We next examined the retina more closely for subtle changes that occur before pit formation. Early in development, shortly before the onset of neurogenesis, we observed that the areas where the foveae will develop are thickened and have a mounded appearance relative to the surrounding retina. This thickening is detected as early as stage 4 in the central retina (data not shown) and by stage 5 in the temporal retina (Figure 2a). By stage 6, these areas become more pronounced as the plexiform layers develop (Figure 2g). It is during this time that ocular elongation begins in the central and temporal regions of the eye (Rasys, Pau, Irwin, Luo, Kim, et al., 2021). These regions will continue to elongate, peaking around stage 14 (Rasys, Pau, Irwin, Luo, Kim, et al., 2021). As this process occurs, the regionalized retinal thickening in the presumptive foveal areas gradually disappears (Figures 2m and 3a,e,i). By stages 9 and 10, regions with a thickened retina are no longer present (Figure 3a,e). Nearing the peak elongation (stage 13), the entire retina has dramatically thinned (Figure 3i). After this point, the eye begins to retract; as it does so, the retina thickens, and pit formation occurs.

To further characterize and quantify alterations to the retina during periods of ocular elongation and retraction, we assessed changes in retina length and thickness in embryos during early retina neurogenesis (stage 6; $n=4$), at the peak of elongation (stage 14; $n=4$), and at hatching ($n=6$). Retinas from each sectioned eye were measured from the temporal to nasal ciliary marginal zones to obtain total retina lengths. Because eye size varies dramatically between these developmental periods, we divided each retina into ten distinct bins to ensure that retina widths, measured at the intersection of each bin, were representative of the same region across different stage embryos. We found that total retina length follows a similar pattern to changes in ocular shape. During early development (stage 6), the mean retinal length is 3706 ± 410 µm. At the peak of ocular elongation, retinal length

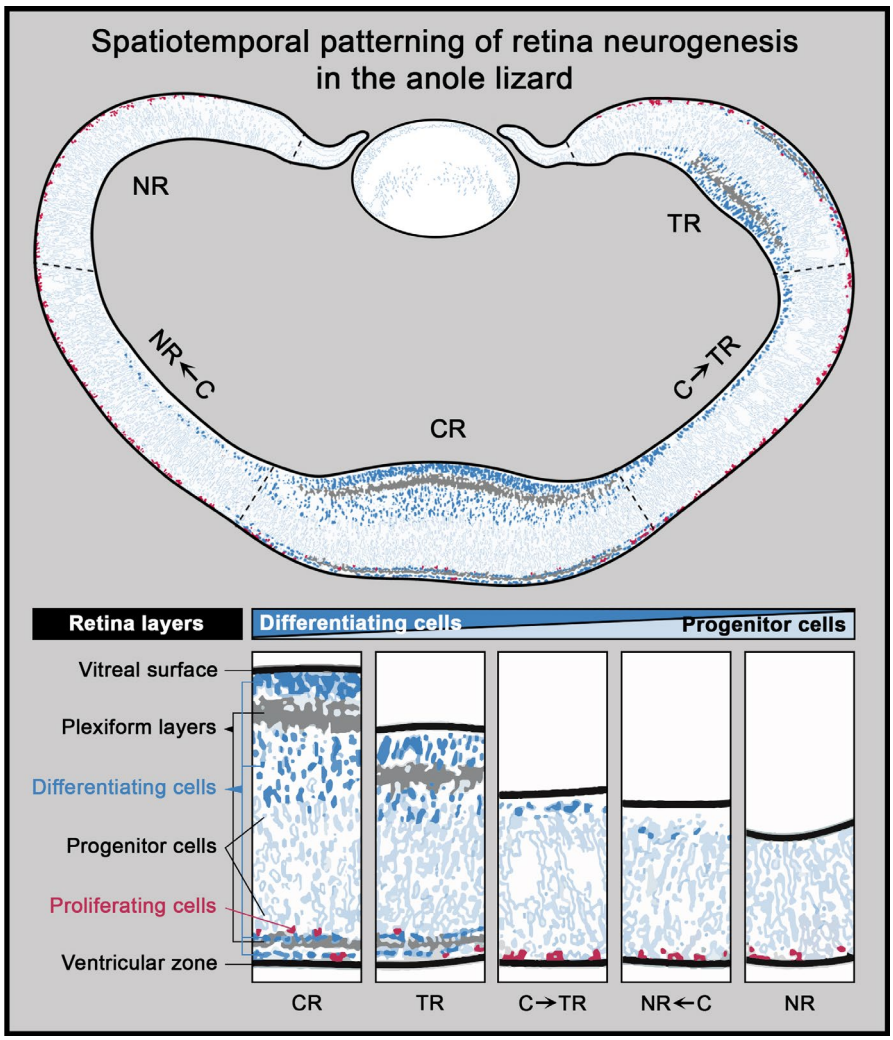

FIGURE 9 Illustration of the anole's spatiotemporal patterning of retina neurogenesis. Retina areas: NR—nasal retina; NR←C—retina region between nasal and central retina; CR—central retina; C→TR—region of the retina between central and temporal areas; TR—temporal retina.

increases to 5063±225 μm. By hatching, when the eye has retracted, retinal length decreases to 3509±90 μm.

Next, we examined retinal thickness distribution across these timepoints (Figure 8). We determined that retinal thickness changes largely as a function of retinal length or the development of the plexiform layers. Although stage 6 and stage 14 embryos have similar overall retinal thickness (Figure 8b,c), at stage 14 the plexiform layers are developed, whereas at stage 6 the retina is still differentiating (Figure 8). As a result, some retinal growth is expected to occur from retinal lamination in the stage 6 embryo. From stage 14 to hatching, retinal thickness dramatically increases through thickening of both the nuclear and plexiform layers (Figure 8c).

4 | DISCUSSION

The fovea is a fascinating structure. Although rare among mammals, it is present in the eyes of several species of birds, reptiles, and fish. Morphological comparisons across these species reveal significant variation in the fovea's structure. In vertebrates that possess a fovea, it can range from a deep, funnel-shaped pit, where most or all retinal cell bodies are laterally displaced, to a shallow depression with only partial displacement of retinal cell bodies.

This diversity raises several intriguing mechanistic questions: Is there an evolutionarily conserved mechanism responsible for creating the foveal pit in all these species, or do different mechanisms act to create different foveal shapes, such as the shallow pit observed in primates and in the temporal retina of lizards and birds compared to the deep central fovea found in birds and lizards? Alternatively, is there a mechanism that functions early in foveal development that is conserved among species, but the formation of either a deep, steep foveal pit or a wide, shallow pit depends on divergent mechanisms? Studies of retinal development in anole lizards, which exhibit both types of foveal structures, can help bridge gaps in understanding foveal development across different vertebrates.

The work we present here shows that foveal regions are morphologically apparent very early on, even before retinal layers are present. We find that differentiation begins first within these regions before the rest of the retina (for illustration see Figure 9). We also provide evidence that ocular elongation occurs shortly after retinal neurogenesis appears complete within these foveal areas. Moreover, consistent with our hypothesis that fovea morphogenesis is driven by remodeling of the retina cell layers, we observed that the retina appears to be influenced by changes in ocular shape and size as well. As the eye elongates, foveal areas progressively thin, and retina thickening is lost. By the point of maximum elongation, when eye size is at its largest, retinal depth is at its thinnest throughout the entire eye. The eye then retracts, at which time retina thickness increases, and remodeling of the retina results in pit formation and photoreceptor cell packing. The timing and sequence of these events—neurogenesis leading to ocular elongation followed by retraction and retinal remodeling (i.e., pit formation and photoreceptor cell packing; for illustration see Figure 10)—suggests that fovea morphogenesis includes a series of steps that begin early and continue throughout most of embryonic development.

Evidence for a relationship between the timing of retinal definition and ocular elongation also exists in humans (Rasys et al., 2024). During early eye development, the macular region, where the fovea will eventually develop, is the site where retinal neurogenesis first begins and concludes. In humans, this happens between 2 and 4 months of gestation in the macular region (Barber, 1955; Barishak, 1992; Hendrickson, 2015; Hendrickson & Provis, 2006; Hendrickson & Zhang, 2017; Hollenberg & Spira, 1972, 1973; Linberg & Fisher, 1990; Mann, 1928; Provis et al., 1985; Rhodes, 1979; van Driel et al., 1990) and between 5 and 7 months in the peripheral retina (Barber, 1955; Hendrickson, 1992, 2015; Hendrickson & Zhang, 2017; Mann, 1928). This 2–4-month time frame is also when asymmetrical changes in ocular shape are observed in human embryonic eyes (Rasys et al., 2024). For instance, a transient bulge develops within the temporal posterior region of the eye where the future fovea will develop, starting at around 2 months and peaking at 4 months (Bach & Seefelder, 1911; Badtke, 1952; Sondermann, 1950; Van & Pilleri, 1961; von Ammon, 1858). This bulge then progressively disappears between 5 and 8 months of gestation (Bach & Seefelder, 1911; Badtke, 1952; Königstein, 1884; Sondermann, 1950; Van & Pilleri, 1961; von Ammon, 1858), overlapping the time frame when pit formation occurs (Hendrickson et al., 2012; Hendrickson & Drucker, 1992; Hendrickson & Yuodelis, 1984; Mann, 1928; Yuodelis & Hendrickson, 1986). This process in humans is gradual and begins with GCL thickening (Hendrickson et al., 2012; Hendrickson & Yuodelis, 1984), followed by pit formation, which slowly increases in depth during the latter months of gestation leading up to birth (Hendrickson et al., 2012, Hendrickson & Yuodelis, 1984). Following this, photoreceptor cells move toward and pack around the fovea center (Hendrickson et al., 2012; Hendrickson & Drucker, 1992; Hendrickson & Yuodelis, 1984; Yuodelis & Hendrickson, 1986).

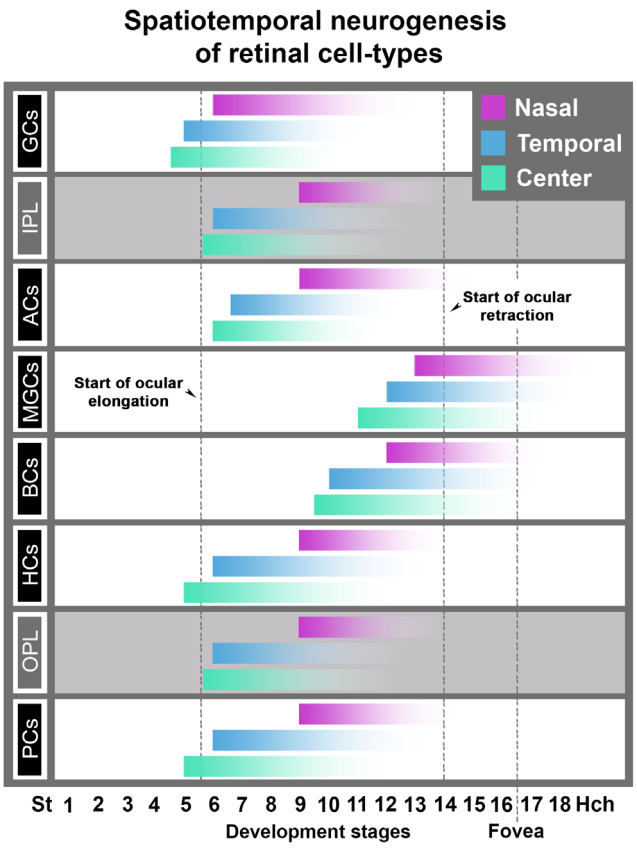

FIGURE 10 Diagram illustrating the emergence of the different retina cell-types in the anole retina. Nasal (magenta), central (cyan), and temporal (blue) retina patterns are illustrated. Dashed lines indicated periods of ocular elongation, retraction, and pit formation.

Given the occurrence of asymmetric changes in globe expansion and retraction, one might expect corresponding regional differences in retinal morphology. For instance, eye elongation occurs to a much greater extent within the central foveal area compared to the temporal area, and the shape of its elongation is also very different (Rasys, Pau, Irwin, Luo, Kim, et al., 2021). One expected outcome is differences in retinal remodeling, such as pit size and photoreceptor cell packing. Consistent with this, we find that the central pit is more pronounced than the temporal fovea, and there is a higher degree of photoreceptor packing in the central fovea. Interestingly, the two foveated areas develop through slightly different sequences of events. In the central fovea, photoreceptor cell packing and retinal lateral displacement occur simultaneously, whereas in the temporal fovea, a localized increase in the number of soma in the GCL occurs first, followed by an increased number of photoreceptor cells and then pit formation.

In humans, ocular elongation encompasses a broad region of the globe. Similar to the anole's temporal fovea, a localized increase in the number of soma in the GCL, which results in a mounded appearance of the GCL, is observed prior to pit formation (Hendrickson et al., 2012, Hendrickson & Yuodelis, 1984). We believe that GCL mounding before pit formation is an indication of ocular retraction, but the degree of mounding is influenced by the overall shape of ocular elongation (Rasys et al., 2024). The distribution of forces differs between the central fovea than the temporal fovea. In the central area, elongation is narrow and funnel-like,

whereas in the temporal region, it is much shallower and broader. Assuming that foveal retinal areas are subjected to equal internal resistance (i.e., intraocular pressure) and possess the same intrinsic properties (i.e., equal elasticity), it is reasonable to expect that mechanical forces exerted at the apex of the elongated regions during retraction would be greater in the central region compared to the temporal. For instance, a broader, elongated region would likely disperse and alleviate some of the forces generated during ocular retraction, whereas a narrower, more confined elongated region would tend to focus them. This could explain why the central and temporal foveal areas are morphologically different in anoles. Chameleons also have a fovea and undergo similar changes in eye shape (Rasys et al., 2024; Rasys, Pau, Irwin, Luo, Kim, et al., 2021). Their central foveal region elongates and retracts to a similar degree as in anoles, but the shape of its elongation is broader than that of the anole's central elongated region. It would be interesting to determine if GCL mounding occurs during central fovea development in chameleons to test the relationship between ocular elongation patterns and localized retinal thickening.

As noted in the introduction, most of our understanding of fovea development comes from histological studies of the primate eye. Therefore, we can compare several morphological aspects of foveal development between *A. sagrei* and haplorhine primates. Although numerous studies have been published on foveal structures in the eyes of adult birds, reptiles, and fish, only one study has included fovea development in birds (zebra finch; Sugiyama et al., 2020) and two studies show some aspects of eye development in seahorses (Novelli et al., 2015; Ofelio et al., 2018). However, these studies are very limited and focus only on later stages when pit formation occurs. Histological sections of the developing zebra finch central fovea (Sugiyama et al., 2020) reveal that its pit develops in a very similar way to the foveae of anoles. The retina starts off very uniform, with no evidence of GCL thickening prior to pit formation, similar to the anole central fovea. The retina then becomes indented, forming the pit as all the retinal cell layers progressively thin and photoreceptor cells begin to pack in around the developing fovea. Interestingly, like the anole's temporal fovea, the zebra finch's central fovea retains all its retinal cell layers. This also appears true for the fovea of seahorses. Histological sections of the eyes of two different juvenile seahorse species (*Hippocampus reidi* and *Hippocampus guttulatus*) at the time of release from the male seahorse's pouch show retinal structures with features similar to the temporal fovea of stage 16 *A. sagrei* embryos: a regionally mounded retina correlating with an apparent increase in the density of soma in the inner nuclear layer (INL) and photoreceptors in the outer nuclear layer (ONL). About 1 month after release from the male seahorse's pouch, *H. guttulatus* juveniles possess a well-defined funnel-like pit (Ofelio et al., 2018). The fovea at this stage of development appears most similar to the temporal fovea in hatchling *A. sagrei*.

Although limited, these comparative observations of fovea development between *A. sagrei*, *Taeniopygia guttata*, and *Hippocampus* suggest that, as with primates, fovea morphogenesis is driven by remodeling of the retinal cell layers. However, because these studies do not capture key periods of early retinal neurogenesis, it is presently unclear whether foveal regions in birds and fish are specified early during retinal development, as they are in anoles and primates. Moreover, since embryonic studies investigating ocular shape are still needed, it will be interesting to explore whether fovea morphogenesis in birds and fish is influenced by changes in ocular shape and size as well.

Our detailed histological and morphological analyses of the anole retina provide a foundation for future experimental approaches. These include gene manipulation techniques to further explore the genetic and molecular pathways involved in fovea formation, potentially shedding light on these processes in a wide range of species. Overall, the research on *Anolis sagrei* not only enhances our understanding of retinal development in this specific lizard but also provides a valuable comparative model that can inform studies on foveal development in primates and other vertebrates.

AUTHOR CONTRIBUTIONS

Ashley M. Rasys: Led the experimental design, data acquisition, and preparation of the manuscript. Shana H. Pau, Shana H. Pau, Katherine E. Irwin, Sherry Luo, Hannah Q. Kim, M. Austin Wahle: Were undergraduate researchers that participated in data collection. Douglas B. Menke and James D. Lauderdale: Obtained funding for the project and participated in experimental design and manuscript preparation.

ACKNOWLEDGMENTS

The authors wish to thank the members of the Lauderdale and Menke research groups—Rebecca Ball, Christina Sabin, Sergio Minchey, Sukhada Samudra, and Aaron Alcala—for their assistance in the care of anole lizards at the University of Georgia. The authors also appreciate and thank Drs. Jonathan Eggenschwiler and Heike Kroeger, as well as Christina Sabin and Sukhada Samudra, for their helpful suggestions and editorial comments on this manuscript. The authors also acknowledge the UGA Honors Program and the Center for Undergraduate Research Opportunities, which supported Ms. Katie Irwin, Ms. Sherry Luo, Ms. M. Austin Wahle, and Ms. Hannah Kim in the form of CURO Summer Fellowships and CURO Research Assistantships.

FUNDING INFORMATION

This work was supported through the National Science Foundation awards 1149453 to D.B.M. and 1827647 to D.B.M. and J.D.L. and a Society for Developmental Biology Emerging Models grant to A.M.R. A.M.R. was supported by NIH NIGMS training grant T32GM007103 and by an ARCS Foundation Scholarship.

CONFLICT OF INTEREST STATEMENT

The authors have nothing to disclose. The funders of this research had no role in study design, data collection and analysis, decision to publish, or preparation of the manuscript.

DATA AVAILABILITY STATEMENT

The data that support the findings of this study are available from the corresponding author upon reasonable request.

ORCID

James D. Lauderdale https://orcid.org/0000-0001-7503-0528

REFERENCES

Association AVM. (2020) *AVMA guidelines for the euthanasia of animals: 2020 Edition*. Schaumburg, IL: American Veterinary Medical Association.

Bach, L. & Seefelder, R. (1911) *Atlas zur Entwicklungsgeschichte des menschlichen Auges*. Leipzig: W. Engelmann. 1914.

Badtke, G. (1952) Entwicklungsmechanische Faktoren bei der Formgebung des embryonalen Augapfels. *Albrecht von Graefe's Archiv für Ophthalmologie*, 152, 671–688.

Barber, A.N. (1955) *Embryology of the human eye*. St. Louis, MO: C. V. Mosby Company.

Barishak, Y.R. (1992) *Embryology of the eye and its adnexa*. Dev Ophthalmol. 24, 1–142.

Beazley, L.D., Perry, V.H., Baker, B. & Darby, J.E. (1987) An investigation into the role of ganglion cells in the regulation of division and death of other retinal cells. *Retinal Development*, 430, 169–184.

Bringmann, A. (2019) Structure and function of the bird fovea. *Anatomia, Histologia, Embryologia*, 48, 177–200.

Collin, S.P. (1999) The foveal photoreceptor mosaic in the pipefish, *Corythoichthyes paxtoni* (Syngnathidae, Teleostei). *Histology and Histopathology*, 14, 369–382.

Conroy, C.J., Papenfuss, T., Parker, J. & Hahn, N.E. (2009) Use of tricaine methanesulfonate (MS222) for euthanasia of reptiles. *Journal of the American Association for Laboratory Animal Science: JAALAS*, 48, 28–32.

Coulombre, A.J. (1955) Correlations of structural and biochemical changes in the developing retina of the chick. *The American Journal of Anatomy*, 96, 153–189.

Easter, S.S., Jr. (1992) Retinal growth in foveated teleosts: nasotemporal asymmetry keeps the fovea in temporal retina. *The Journal of Neuroscience*, 12, 2381–2392.

Fite, K.V. & Lister, B.C. (1981) Bifoveal vision in anolis lizards. *Brain, Behavior and Evolution*, 19, 144–154.

Fite, K.V. & Rosenfield-Wessels, S. (1975) A comparative study of deep avian foveas. *Brain, Behavior and Evolution*, 12, 97–115.

Fleishman, L.J. (2024) Lizard visual ecology. *Frontiers in Amphibian and Reptile Science*, 2, 1426675.

Hendrickson, A. (1992) A morphological comparison of foveal development in man and monkey. *Eye (London, England)*, 6(Pt 2), 136–144.

Hendrickson, A. (2005) Organization of the adult primate fovea. In: Penfold, P.L. & Provis, J.M. (Eds.) *Macular degeneration*. Berlin, Heidelberg: Springer Berlin Heidelberg, pp. 1–23.

Hendrickson, A. (2015) Development of retinal layers in prenatal human retina. *American Journal of Ophthalmology*, 166, 29–35.

Hendrickson, A. & Drucker, D. (1992) The development of parafoveal and mid-peripheral human retina. *Behavioural Brain Research*, 49, 21–31.

Hendrickson, A. & Kupfer, C. (1976) The histogenesis of the fovea in the macaque monkey. *Investigative Ophthalmology & Visual Science*, 15, 746–756.

Hendrickson, A., Possin, D., Vajzovic, L. & Toth, C.A. (2012) Histologic development of the human fovea from midgestation to maturity. *American Journal of Ophthalmology*, 154, 767–778.e2.

Hendrickson, A. & Provis, J. (2006) *Comparison of development of the primate fovea centralis with peripheral retina*(Harris, B., Sernagor, E., Wong, R. and Eglen, S. (Eds.)). Cambridge: Cambridge University Press, pp. 126–149.

Hendrickson, A. & Zhang, C. (2017) Development of cone photoreceptors and their synapses in the human and monkey fovea. *The Journal of Comparative Neurology*, 527, 38–51.

Hendrickson, A.E. & Yuodelis, C. (1984) The morphological development of the human fovea. *Ophthalmology*, 91, 603–612.

Hollenberg, M.J. & Spira, A.W. (1972) Early development of the human retina. *Canadian Journal of Ophthalmology*, 7, 472–491.

Hollenberg, M.J. & Spira, A.W. (1973) Human retinal development: ultrastructure of the outer retina. *American Journal of Anatomy*, 137, 357–385.

Hulke, J.W. (1866) On the chameleon's retina; a further contribution to the minute anatomy of the retina of reptiles. *Philosophical Transactions of the Royal Society of London*, 156, 223–229.

Kahn, A.J. (1974) An autoradiographic analysis of the time of appearance of neurons in the developing chick neural retina. *Developmental Biology*, 38, 30–40.

Königstein, L. (1884) Histiologische Notizen. *Albrecht von Graefe's Archiv für Ophthalmologie*, 30, 135–144.

La Vail, M.M., Rapaport, D.H. & Rakic, P. (1991) Cytogenesis in the monkey retina. *The Journal of Comparative Neurology*, 309, 86–114.

Linberg, K.A. & Fisher, S.K. (1990) A burst of differentiation in the outer posterior retina of the eleven-week human fetus: an ultrastructural study. *Visual Neuroscience*, 5, 43–60.

Locket, N.A. (1992) Problems of deep foveas. *Australian and New Zealand Journal of Ophthalmology*, 20, 281–295.

Makaretz, M. & Levine, R.L. (1980) A light microscopic study of the bifoveate retina in the lizard Anolis carolinensis: general observations and convergence ratios. *Vision Research*, 20, 679–686.

Mann, I.C. (1928) *The development of the human eye*. Cambridge, UK: The University Press.

Mitkus, M., Potier, S., Martin, G.R., Duriez, O. & Kelber, A. (2018) *Raptor vision*. New York: Oxford University Press.

Novelli, B., Socorro, J.A., Caballero, M.J., Otero-Ferrer, F., Segade-Botella, A. & Molina Dominguez, L. (2015) Development of seahorse (*Hippocampus reidi*, Ginsburg 1933): histological and histochemical study. *Fish Physiology and Biochemistry*, 41, 1233–1251.

Ofelio, C., Diaz, A.O., Radaelli, G. & Planas, M. (2018) Histological development of the long-snouted seahorse *Hippocampus guttulatus* during ontogeny. *Journal of Fish Biology*, 93, 72–87.

O'Rahilly, R. & Meyer, D.B. (1959) The early development of the eye in the chick *Gallus domesticus* (stages 8 to 25). *Acta Anatomica*, 36, 20–58.

Peng, Y.R., Shekhar, K., Yan, W., Herrmann, D., Sappington, A., Bryman, G.S. et al. (2019) Molecular classification and comparative Taxonomics of foveal and peripheral cells in primate retina. *Cell*, 176, 1222–1237.e22.

Prada, C., Puga, J., Perez-Mendez, L., Lopez, R. & Ramirez, G. (1991) Spatial and temporal patterns of neurogenesis in the Chick Retina. *The European Journal of Neuroscience*, 3, 559–569.

Provis, J.M., van Driel, D., Billson, F.A. & Russell, P. (1985) Development of the human retina: patterns of cell distribution and redistribution in the ganglion cell layer. *The Journal of Comparative Neurology*, 233, 429–451.

Rasys, A.M., Divers, S.J., Lauderdale, J.D. & Menke, D.B. (2019) A systematic study of injectable anesthetic agents in the brown anole lizard (*Anolis sagrei*). *Laboratory Animals*, 54, 281–294.

Rasys, A.M., Park, S., Ball, R.E., Alcala, A.J., Lauderdale, J.D. & Menke, D.B. (2019) CRISPR-Cas9 gene editing in lizards through microinjection of unfertilized oocytes. *Cell Reports*, 28, 2288.

Rasys, A.M., Pau, S.H., Irwin, K.E., Luo, S., Kim, H.Q., Wahle, M.A. et al. (2021) Ocular elongation and retraction in foveated reptiles. *Developmental Dynamics*, 250, 1584–1599.

Rasys, A.M., Pau, S.H., Irwin, K.E., Luo, S., Menke, D.B. & Lauderdale, J.D. (2021) Anterior eye development in the brown anole, *Anolis sagrei*. *bioRxiv*, 1–21. https://doi.org/10.1101/2021.02.15.429783

Rasys, A.M., Wegerski, A., Trainor, P.A., Hufnagel, R.B., Menke, D.B. & Lauderdale, J.D. (2024) Dynamic changes in ocular shape during human development and its implications for retina fovea formation. *BioEssays*, 46, e2300054.

Rhodes, R.H. (1979) A light microscopic study of the developing human neural retina. *The American Journal of Anatomy*, 154, 195–209.

Röll, B. (2001) Gecko vision—retinal organization, foveae and implications for binocular vision. *Vision Research*, 41, 2043–2056.

Sanger, T.J., Hime, P.M., Johnson, M.A., Diani, J. & Losos, J.B. (2008) Laboratory protocols for husbandry and embryo collection of Anolis lizards. *Herpetological Review*, 39, 58–63.

Sanger, T.J., Losos, J.B. & Gibson-Brown, J.J. (2008) A developmental staging series for the lizard genus Anolis: a new system for the integration of evolution, development, and ecology. *Journal of Morphology*, 269, 129–137.

Sannan, N.S., Shan, X., Gregory-Evans, K., Kusumi, K. & Gregory-Evans, C.Y. (2018) Anolis carolinensis as a model to understand the molecular and cellular basis of foveal development. *Experimental Eye Research*, 173, 138–147.

Slonaker, J.R. (1897) A comparative study of the area of acute vision in vertebrates. *Journal of Morphology*, 13, 445–502.

Smith, R.S., John, S.W.M., Nishina, P.M. & Sundberg, J.P. (2001) *Systematic evaluation of the mouse eye*. London, UK: CRC Press.

Sondermann, R. (1950) Die bedeutung der vererbung für die entwicklung der myopie. *Albrecht von Graefes Archiv für Klinische und Experimentelle Ophthalmologie*, 151, 200–208.

Springer, A.D. & Hendrickson, A.E. (2004a) Development of the primate area of high acuity. 1. Use of finite element analysis models to identify mechanical variables affecting pit formation. *Visual Neuroscience*, 21, 53–62.

Springer, A.D. & Hendrickson, A.E. (2004b) Development of the primate area of high acuity. 2. Quantitative morphological changes associated with retinal and pars plana growth. *Visual Neuroscience*, 21, 775–790.

Springer, A.D. & Hendrickson, A.E. (2005) Development of the primate area of high acuity, 3: temporal relationships between pit formation, retinal elongation and cone packing. *Visual Neuroscience*, 22, 171–185.

Sugiyama, T., Yamamoto, H., Kon, T., Chaya, T., Omori, Y., Suzuki, Y. et al. (2020) The potential role of Arhgef33 RhoGEF in foveal development in the zebra finch retina. *Scientific Reports*, 10, 21450.

Underwood, G. (1970) The eye. In: Gans, C. & Parsons, T.S. (Eds.) *Biology of the reptilia, volume 2. Morphology B*. London and New York: Academic Press, Inc, pp. 1–93.

van Driel, D., Provis, J.M. & Billson, F.A. (1990) Early differentiation of ganglion, amacrine, bipolar, and Muller cells in the developing fovea of human retina. *Journal of Comparative Neurology*, 291, 203–219.

Van, L. & Pilleri, G. (1961) Morphological research on the "scleral protuberance". *Albrecht von Graefe's Archiv für Ophthalmologie*, 163, 1–9.

Voigt, A.P., Whitmore, S.S., Flamme-Wiese, M.J., Riker, M.J., Wiley, L.A., Tucker, B.A. et al. (2019) Molecular characterization of foveal versus peripheral human retina by single-cell RNA sequencing. *Experimental Eye Research*, 184, 234–242.

von Ammon, F.A. (1858) Die entwicklungsgeschichte des menschlichen auges. *Graefe's Archiv für Ophthalmologie*. Berlin, Germany: Springer-Verlag.

Wahle, M.A., Kim, H.Q., Menke, D.B., Lauderdale, J.D. & Rasys, A.M. (2023) Maturation and refinement of the maculae and foveae in the Anolis sagrei lizard. *Experimental Eye Research*, 234, 109611.

Walls, G.L. (1942) *The vertebrate eye and its adaptive radiation*. Bloomfield Hills, Michigan: The Cranbrook Institute of Science.

Weysse, A.W. & Burgess, W.S. (1906) Histogenesis of the retina. *The American Naturalist*, 40, 611–637.

Yan, W., Peng, Y.R., van Zyl, T., Regev, A., Shekhar, K., Juric, D. et al. (2020) Cell atlas of the human fovea and peripheral retina. *Scientific Reports*, 10, 9802.

Yuodelis, C. & Hendrickson, A. (1986) A qualitative and quantitative analysis of the human fovea during development. *Vision Research*, 26, 847–855.

How to cite this article: Rasys, A.M., Pau, S.H., Irwin, K.E., Luo, S., Kim, H.Q., Wahle, M.A. et al. (2025) Histological analysis of retinal development and remodeling in the brown anole lizard (*Anolis sagrei*). *Journal of Anatomy*, 246, 1019–1033. Available from: https://doi.org/10.1111/joa.14193